

**Coupled plasmon resonances in monolayers of metal nanoparticles and nanoshells**

Boris N. Khlebtsov

*Institute of Biochemistry and Physiology of Plants and Microorganisms, Russian Academy of Sciences, 13 Prospekt Entuziastov, Saratov 410049, Russia*

Vitaliy A. Khanadeyev

*Saratov State University, 155 Ulitsa Moskovskaya, Saratov 410026, Russia*

Jian Ye

*Interuniversity Microelectronics Center (IMEC), Kapeldreef 75, 3001 Leuven, Belgium*

Daniel W. Mackowski

*Mechanical Engineering Department, Auburn University, Alabama 36849, USA*

Gustaaf Borghs

*Interuniversity Microelectronics Center (IMEC), Kapeldreef 75, 3001 Leuven, Belgium*

Nikolai G. Khlebtsov\*

*Institute of Biochemistry and Physiology of Plants and Microorganisms, Russian Academy of Sciences, 13 Prospekt Entuziastov, Saratov 410049, Russia and Saratov State University, 155 Ulitsa Moskovskaya, Saratov 410026, Russia*

(Received 20 November 2007; revised manuscript received 26 December 2007; published 31 January 2008)

We report on the coupled plasmon resonances in a monolayer consisting of metal or metalodielectric nanoparticles with the dipole and quadrupole single-particle resonances. The theoretical models included spherical gold and silver particles and also gold and silver nanoshells on silica and polystyrene cores forming two dimensional random clusters or square-lattice arrays on a dielectric substrate (glass in water). The parameters of the individual particles were chosen so that a quadrupole plasmon resonance could be observed along with the dipole-scattering band. By using an exact multipole cluster-on-a-substrate solution, we showed that particle-substrate coupling can be neglected in the calculation of the monolayer-extinction spectra, at least for the glass-in-water configuration. When the surface particle density in the monolayer was increased, the dipole resonance became suppressed and the spectrum for the cooperative system was determined only by the quadrupole plasmon. The dependence of this effect on the single-particle parameters and on the cluster structure was examined in detail. In particular, the selective suppression of the long-wavelength extinction band was shown to arise from the cooperative suppression of the dipole-scattering mode, whereas the short-wavelength absorption spectrum for the monolayer was shown to be little different from the single-particle spectrum. For experimental studies, the silica/gold-nanoshell monolayers were fabricated by the deposition of nanoshells on a glass substrate functionalized by silane-thiol cross-linkers. The measured single-particle and monolayer-extinction spectra are in reasonable agreement with simulations based on the nanoshell geometrical parameters (scanning electron microscopy data). Finally, we evaluated the sensitivity of the coupled quadrupole resonance to the dielectric environment to show a universal linear relation between the relative shift in the coupled-quadrupole-resonance wavelength and the relative increment in the environment refractive index.

DOI: [10.1103/PhysRevB.77.035440](https://doi.org/10.1103/PhysRevB.77.035440)

PACS number(s): 78.67.Bf, 73.20.Mf, 36.40.Vz

**I. INTRODUCTION**

Gold and silver nanoparticles conjugated to biospecific macromolecules are very important for current nanobiotechnology. Their use for analytical purposes,<sup>1</sup> cellular-structure visualization,<sup>2</sup> targeted drug delivery,<sup>3</sup> and photothermal cancer therapy<sup>4</sup> is based on a combination of biological recognition (the probe molecule+the target molecule) and resonance absorption or scattering of light on frequencies corresponding to the excitation of localized plasmons.<sup>5</sup> The spectral tuning of the single-particle plasmon resonances and the change in the ratio between absorption and scattering efficiencies are achieved by varying the particle size, shape, and structure.<sup>6,7</sup>

Along with individual particles, interacting-particle ensembles, including bispheres,<sup>8,9</sup> linear chains,<sup>10</sup> two-dimensional (2D) arrays,<sup>11</sup> and three-dimensional (3D) aggregates,<sup>12</sup> are of much theoretical and practical interest.<sup>13</sup> This paper focuses on the optical properties of 2D arrays fabricated by self-assembly on substrates or by nanolithography.<sup>14</sup> Such nanostructures are used as chemical<sup>15</sup> or biological<sup>1,16</sup> sensors based on the dependence of their optical properties on the dielectric environment.

Recently, Malynych and Chumanov found an unusual behavior of the extinction spectra for a monolayer of interacting silver nanoparticles embedded in a polymer film<sup>17(a)</sup> and examined the dependence of the spectra on the environment refractive index.<sup>17(b)</sup> Specifically, they showed an intense

sharpening of the quadrupole extinction peak resulting from selective suppression of the coupled dipole mode as the interparticle distance becomes smaller. This phenomenon was explained qualitatively by using simple symmetry considerations.<sup>17(a)</sup> It should be noted here that the terms “coupled quadrupole mode” and “coupled dipole mode” mean the spectral location of the coupled extinction bands near the corresponding single-particle dipole and quadrupole resonances. In other words, these terms designate the spectral position of weakly interacting dipole-quadrupole particles when they are far apart. In the general case, however, the extinction bands of closely packed particles result from many multipole contributions (see, e.g., simulations for gold and silver bispheres<sup>9</sup>).

To the best of our knowledge, no extension of the observations in Ref. 17 to nanoshell monolayers has been published, except for our preliminary report.<sup>18</sup> Quite recently, Wang *et al.*<sup>19</sup> showed that the nanoshell array substrates provide a new, multifunctional platform for chemical sensing applications by enhancing both Raman scattering and infrared absorption spectroscopy. However, in contrast to our findings, those authors demonstrated the appearance of an increased near-infrared band rather than its suppression.

Although there is an extensive literature on the optical properties of 2D arrays,<sup>6,12,20–22</sup> it is difficult to extract the general features because of significant variations in the particle and array parameters and in experimental or simulation conditions. For a qualitative understanding of the optical properties of nanoparticle assemblies, it is instructive to consider two coupled small metal nanospheres.<sup>8,9</sup> If the exciting electric field is perpendicular to the bisphere axis, the coupled extinction spectrum is close to the single-particle spectrum, except for a small blueshifting of the extinction peak. In contrast, excitation along the bisphere axis results in a dramatic increase in and a redshifting of the coupled resonance.<sup>9</sup> Furthermore, an accurate calculation of this redshifting effect requires the inclusion of several multipole orders, even if each component sphere is, individually, well within the dipole approximation.<sup>9,23</sup> Thus, the extinction spectrum is polarization dependent and the coupled dipole model cannot predict the bisphere spectrum exactly. In what follows, we shall consider arrays under unpolarized light, with the resultant spectrum being the superposition of two independent polarization contributions. Accordingly, for bispheres, there are two extinction bands, one of which is minor and close to the single-particle resonance and the other is more intensive and is more or less redshifted, depending on the particle separation.

For a 2D lattice array of double-layered touching 15 nm gold particles covered by a thin (0.125 nm) dielectric layer, our  $T$  matrix simulations<sup>13</sup> predicted a redshifted and broadened extinction band located near 700 nm. Calculations by Zhao *et al.*<sup>11</sup> for lattice arrays of 60 nm silver particles showed that (a) the plasmon wavelength blueshifts as the array spacing ( $D$ ) decreases for  $D$  larger than 75 nm and then redshifts for smaller distances and that (b) the plasmon width narrows for  $D > 180$  nm but broadens for smaller distances. In regard to the goals of the present work, a more important observation of Ref. 11 is the general decrease in the coupled extinction band with decreasing interparticle separation.

However, we have not found any additional published experimental data apart from those reported in Refs. 17–19. We are also unaware of detailed multipole computations that explain the cooperative optical properties of 2D arrays of double-layered particles possessing a dipole and a quadrupole single-particle resonance except for Refs. 21 and 24 (on nanoshell dimers) and our preliminary report.<sup>18</sup> This lack of understanding of coupled effects has also been recognized by Malynych and Chumanov,<sup>17(a)</sup> who wrote the following: “The excitation of the coupled plasmon modes corresponds to the simultaneous interaction of several particles with light; however, it is not clear what the coherence length is or what the minimum number of particles required to establish the observed narrow band is.”

This work was aimed at investigating the following questions:

(1) Is it possible to experimentally observe the effect described in Ref. 17 for nanoparticles other than silver spheres, e.g., for monolayers of gold nanoshells of the  $\text{SiO}_2(\text{core})/\text{Au,Ag}(\text{shell})$  or polystyrene(*core*)/ $\text{Au,Ag}(\text{shell})$  type?

(2) How is the suppression of the coupled dipole mode dependent on particle parameters (metal type, nanosphere size, or core and shell sizes) and on array structure (minimal number of particles in an ensemble, lattice period, average density in a random cluster, etc.)?

(3) Is there a correlation between the cooperative behavior of a 2D ensemble of nanoshells and their absorption and scattering efficiencies?

(4) How does the coupled-quadrupole-resonance wavelength depend on the dielectric environment, including substrate properties?

This paper presents exact multipole simulations for dipole-quadrupole plasmon-resonant particles on a dielectric interface.

## II. THEORY

### A. Calculation models and methods

#### 1. Particles and two-dimensional arrays in a homogeneous dielectric medium

We modeled the optical properties of monolayers built up from five types of particles: (1) silver and gold nanospheres of diameters  $d_{\text{Ag}}$  and  $d_{\text{Au}}$ , (2) gold nanoshells with a silica core of diameter  $d_{\text{SiO}_2}$  and external diameter  $d_{\text{Au}}$  [nanoshell thickness  $\Delta d_{\text{Au}} = (d_{\text{Au}} - d_{\text{SiO}_2})/2$ ], (3) silver nanoshells with a silica core of diameter  $d_{\text{SiO}_2}$  and external diameter  $d_{\text{Ag}}$  [nanoshell thickness  $\Delta d_{\text{Ag}} = (d_{\text{Ag}} - d_{\text{SiO}_2})/2$ ], and [(4) and (5)] gold and silver nanoshells with polystyrene cores.

As a simple monolayer model, we used a square lattice with a period

$$p = d_e(1 + s), \quad (1)$$

where  $d_e$  is the external diameter and  $s$  is the relative interparticle distance. Another monolayer model was obtained by randomly filling a square of side  $L/d_e$  with a given number of particles  $N$ . Then, the relative coordinates of the particles  $X_i$  were transformed as

$$x_i = X_i d_e (1 + s), \quad (2)$$

where the parameter  $s$  controls the minimal interparticle distance. The structure of the resultant monolayer is characterized by the particle number  $N$  and the average surface particle density

$$\rho = NS_{geom} [L^2(1+s)^2]. \quad (3)$$

Apparently, for a lattice cluster, we have  $\rho = (\pi/4)/(1+s)^2$ .

## 2. Calculation of the absorption and scattering spectra

The spectral dependences of the refractive indices for water and silica were calculated from the formulas given in Ref. 25. The optical dielectric function of gold  $\epsilon_{Au}$  was computed from a spline as described in Ref. 25, with the slight modification that for wavelengths ranging from 620 to 1600 nm, the tabulated data of Ref. 26 were used. The dielectric function of the silver spline was obtained from the data of Ref. 26. For solid nanospheres, no size correction to  $\epsilon_{Au,Ag}$  was needed because the particle diameter was greater than 50 nm. For gold and silver nanoshells, however,  $\epsilon_{Au,Ag}$  were corrected for the diffuse surface scattering of electrons at the nanoshell boundaries, as described in Ref. 27.

The extinction, scattering, and absorption cross sections for isolated particles were normalized to the geometrical cross section  $S_{geom}$  ( $Q_{ext,sca,abs} = C_{ext,sca,abs}/S_{geom}$ ) and were calculated by the usual Mie theory formulas<sup>28</sup> for nanospheres and by the recursive formulas given in Ref. 29 for nanoshells.

The optical properties of the monolayers were described in terms of normalized cross sections,

$$Q_{ext,sca,abs} = C_{ext,sca,abs}/NS_{geom}, \quad (4)$$

where  $N$  is the number of particles per layer. The cross sections themselves were calculated from the generalized multiparticle Mie (GMM) theory<sup>30</sup> for a system of  $N$  interacting multilayered particles illuminated by unpolarized light. A detailed description of the GMM solution can be found elsewhere (see, e.g., Ref. 30 and references therein). The total field  $\mathbf{E}_{exc}^i$  exciting an  $i$ th cluster particle and the individual scattered field  $\mathbf{E}_{sca}^i$  can be represented as expansions in terms of the regular vector spherical harmonics (VSH) of the first kind,  $\mathbf{Y}_{mnp}^{(1)}$ , centered about the origin of each sphere:

$$\mathbf{E}_{exc}^i \equiv \mathbf{E}_0 + \sum_{j \neq i} \mathbf{E}_{sca}^j = \sum_{\nu} q_{\nu}^i \mathbf{Y}_{\nu}^{(1)}(\mathbf{r} - \mathbf{r}_i), \quad (5)$$

where  $\mathbf{E}_0$  is the incident plane wave,  $\mathbf{r}_i$  is the position vector of the  $i$ th sphere, and the Greek subscripts  $\mu$  and  $\nu$  are shorthand for degree, order, mode, i.e.,  $\mu = (m, n, p)$ . In the same line, the scattered fields can be represented by the outgoing VSH ( $\mathbf{Y}_{mnp}^{(3)}$ ) expansions,

$$\mathbf{E}_{sca}^j(\mathbf{r}) = \sum_{\nu} a_{\nu}^j \mathbf{Y}_{\nu}^{(3)}(\mathbf{r} - \mathbf{r}_j). \quad (6)$$

Application of boundary conditions leads to the generalized Mie theory through the following simple expressions for scattered-field coefficients:<sup>30</sup>

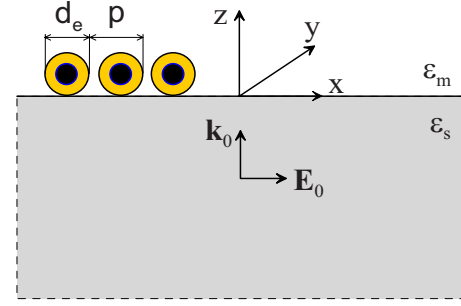


FIG. 1. (Color online) The coordinate system for the exact CSS solution. The incident light propagates in the  $+z$  direction from a half-infinite substrate (the dielectric function  $\epsilon_s$ ) to a half-infinite homogeneous medium ( $\epsilon_m$ ) surrounding two-layered 2D-cluster particles.

$$a_{mnp}^i = \bar{a}_{np}^i q_{mnp}^i, \quad p = 1, 2, \quad (7)$$

where  $\bar{a}_{n1}^i = a_n^i$  and  $\bar{a}_{n2}^i = b_n^i$  are the usual Mie coefficients for an isolated  $i$ th sphere.<sup>28</sup> The exciting coefficients  $q_{\nu}^i$  or, equivalently, the scattering coefficients  $a_{mnp}^i$  can be found from a system of coupled linear equations,

$$\frac{1}{\bar{a}_{\nu}^i} a_{\nu}^i - \sum_{\substack{j=1, \\ j \neq i}}^N \sum_{\mu} H_{\nu\mu}^{ij} a_{\mu}^j = p_{\nu}^i, \quad (8)$$

where  $p_{mnp}^i$  are the known expansion coefficients of the incident field about the origin of the  $i$ th sphere,

$$p_{\nu}^i = p_{\nu} \exp(i\mathbf{k}_0 \cdot \mathbf{r}_i), \quad \mathbf{E}_0(\mathbf{r}) = \sum_{\nu} p_{\nu} \mathbf{Y}_{\nu}^{(1)}(k\mathbf{r}), \quad (9)$$

and the interaction matrix  $H_{\nu\mu}^{ij}$  is determined by the coefficients of VSH translation.<sup>30</sup> After appropriate truncation, we can solve Eq. (8) to find the multipole expansion coefficients  $a_{mnp}^i$ , which determine all light-scattering cluster properties. For example, the extinction cross section can be calculated by the equation

$$C_e = \frac{4\pi}{k^2} \sum_{i=1}^N \sum_{\nu} c_{\nu} \text{Re}[a_{\nu}^i (p_{\nu}^i)^*], \quad (10)$$

where  $k = 2\pi\epsilon_m^{1/2}/\lambda$  is the wave number in the medium,  $\epsilon_m$  is the dielectric function of the medium (in this case, water),  $c_{\nu}$  is the normalization constant, and the asterisk denotes complex conjugation. In practical calculations, the exactness of the solution was checked by the convergence of the calculated spectra obtained with increasing order of multipoles.

## 3. Monolayer on a dielectric substrate

We consider a 2D array of  $N$  spheres or nanoshells on a dielectric surface, which is characterized by a dielectric function  $\epsilon_s$  and is located at a position  $z=0$  below a half-infinite dielectric medium  $\epsilon_m$  (the outward normal points in the  $+z$  direction, Fig. 1). The computational complexity of the problem, even for a single sphere, has led to the development of an approximate solution,<sup>31</sup> which can be referred to as a normal incidence approximation (NIA). The NIA assumes

the reflected field to be produced by a “mirror image” source, so that each sphere interacts primarily with near-normal reflected radiation.

An exact cluster-on-a-surface solution (CSS) has been developed by Mackowski<sup>32</sup> through an extension of the previous solution by Wriedt and Doicu<sup>33</sup> for a single sphere at a surface (see also discussion<sup>32</sup> of the CSS developed by Denti *et al.*<sup>34</sup> and application of the discrete sources method to the scattering by a particle on a plane surface<sup>35</sup>). For CSS details, the readers are referred to Ref. 32; here, we restrict ourselves to a short summary.

The total field  $\mathbf{E}_{exc}^i$  exciting the  $i$ th cluster particle is represented by the sum of the direct ( $\mathbf{E}_{0,d}^i$ ) and reflected ( $\mathbf{E}_{0,r}^i$ ) incident plane waves and by the sum of the directly scattered waves  $\mathbf{E}_{sca,d}^j$  originating from all  $N-1$  spheres, along with the scattered waves that reflect off the surface,  $\mathbf{E}_{sca,r}^j$ :

$$\mathbf{E}_{exc}^i = \mathbf{E}_{0,d}^i + \mathbf{E}_{0,r}^i + \sum_{j=1}^N [(1 - \delta_{ij})\mathbf{E}_{sca,d}^j + \mathbf{E}_{sca,r}^j]. \quad (11)$$

The incident direct ( $\mathbf{E}_{0,d}^i$ ) and reflected ( $\mathbf{E}_{0,r}^i$ ) fields can be represented by Eq. (9), with the expansion coefficients  $p_\nu$  and  $g_\nu$ , respectively. The scattered direct and reflected fields are represented by the outgoing VSH  $\mathbf{Y}_\nu^{(3)}(\mathbf{r}-\mathbf{r}_j)$  expansions, centered about the origin of each sphere. Application of VSH translation theorems for scattered and reflected fields and boundary conditions leads to the following interaction equations:<sup>32</sup>

$$\frac{1}{a_\nu^i} a_\nu^i - \sum_{j=1}^N \sum_{\mu} H_{\nu\mu}^{ij} a_\mu^j - \sum_{j=1}^N \sum_{\mu} R_{\nu\mu}^{ij} a_\mu^j = p_\nu^i + g_\nu^i, \quad (12)$$

where  $R_{\nu\mu}^{ij}$  is the transformation matrix<sup>32</sup> that gives a regular VSH expansion (about the origin  $\mathbf{r}_i$ ) produced by the reflection of the outgoing VSH centered at  $\mathbf{r}_j$ . After appropriate truncation and numerical solution of Eq. (12), the absorption and scattering cross sections of the cluster spheres and the far-field scattering pattern can be calculated as described in Ref. 32.

## B. Calculated results

### 1. Dipole-quadrupole spectra of isolated particles

To observe the suppression of the dipole mode in a 2D ensemble, one should choose the isolated-particle parameters so that both resonances have noticeable intensity. Therefore, we first calculated in detail the spectra for all the models mentioned above and found optimal parameters for the positions and intensities of the quadrupole and dipole modes at wavelengths ranging from 600 to 1100 nm. For example, Fig. 2 shows the spectra for gold nanoshells of the  $\text{SiO}_2/\text{Au}$  type. The shell thicknesses  $\Delta d=15, 20,$  and  $25$  nm correspond to the typical values for our experimental conditions.<sup>36</sup> It can be seen that for these thicknesses, the minimal optimal core diameter  $d$  is approximately 150 nm. For core diameters greater than 200 nm, the dipole-resonance peak is located in the IR region.

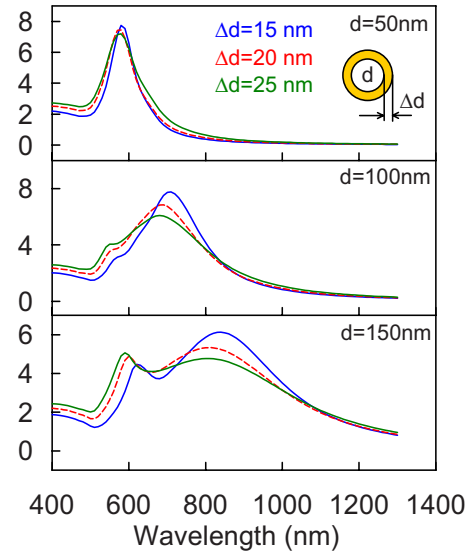


FIG. 2. (Color online) Extinction spectra for  $\text{SiO}_2/\text{Au}$ -type nanoshells with gold-shell thicknesses of 15, 20, and 25 nm and with core diameters of 50, 100, and 150 nm.

### 2. Exact simulations of the particle-substrate coupling effects

In our experiments, particles were deposited onto a 0.1 mm glass substrate, which was then placed in a cuvette with water for spectral measurements. As the substrate thickness was 2 orders higher than the maximal wavelength, a half-infinite substrate model (Fig. 1) seemed adequate for experimental conditions. Furthermore, as the substrate/medium refractive index ratio was about  $1.48/1.33 \approx 1.11$ , it was reasonable to expect small substrate effects on both simulated and measured monolayer spectra. Figure 3 shows an example for 100 nm solid silver spheres placed on a  $6 \times 6$  square lattice and separated by 50 nm distances. Because of the strong interaction among particles, the coupled extinction spectrum demonstrates suppression of the dipole mode.

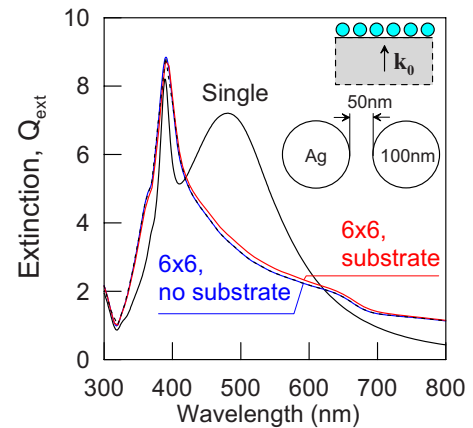


FIG. 3. (Color online) Extinction spectra of a  $6 \times 6$  lattice array of 100 nm silver spheres assembled on a glass substrate ( $n_s = \sqrt{\epsilon_s} = 1.48$ ) in water and separated by 50 nm distances. Calculations are by the exact CSS solution and without the substrate (the same array in water). The single-particle spectrum is shown for comparison.

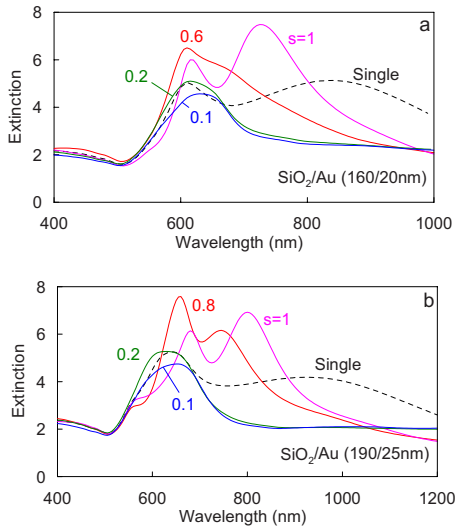


FIG. 4. (Color online) Extinction spectra for  $4 \times 4$  lattice clusters built up from  $\text{SiO}_2/\text{Au}$ -type nanoshells with sizes of (a) 160/20 nm and (b) 190/25 nm. The relative interparticle-distance parameter  $s$  was varied from 1 to 0.1.

More importantly, the glass substrate does give a negligible contribution to the simulated spectrum, as expected from the above arguments and approximate calculations based on a simplified “dipole mirror image” model.<sup>37</sup> Moreover, we found that the NIA differed from the exact results by 1% or 2%. With this in mind, we shall further consider only off-substrate simulations.

### 3. Dependence of the monolayer-extinction spectrum on the interparticle distance

The interparticle distance is a crucial parameter determining the electrodynamic particle coupling and the cooperative spectral properties of an ensemble.<sup>6,11</sup> Therefore, we first investigated the influence of the interparticle-distance parameter  $s$  on the suppression of the dipole mode. The particle parameters corresponded to the experiments discussed in Sec. III. Figure 4(a) illustrates the changes occurring in the extinction spectrum for a  $4 \times 4$  lattice cluster built up from  $\text{SiO}_2/\text{Au}$  nanoshells with a core diameter of 160 nm and a gold-layer thickness of 20 nm as the  $s$  parameter decreases from 1 to 0.1. Beginning with parameter  $s$  values of about 0.2, there was effective suppression of the dipole mode, so that the resonance was determined by only the quadrupole mode at about 610 nm. A twofold decrease in the  $s$  parameter (to as low as 0.1) brought about little change in the system’s spectrum. These conclusions are general and depend little on the properties of the particles themselves. To illustrate, Fig. 4(b) shows the spectra for nanoshells with parameters of 190/25 nm. For  $s$  values of 1 and 0.8, the cluster spectrum exhibits interference structure, possibly related to the idealized array model. Nevertheless, for the low  $s$  values of 0.2 and 0.1, the pattern of dipole-mode suppression is similar to that in Fig. 4(a). This conclusion holds for silver particles and nanoshells as well (data not shown).

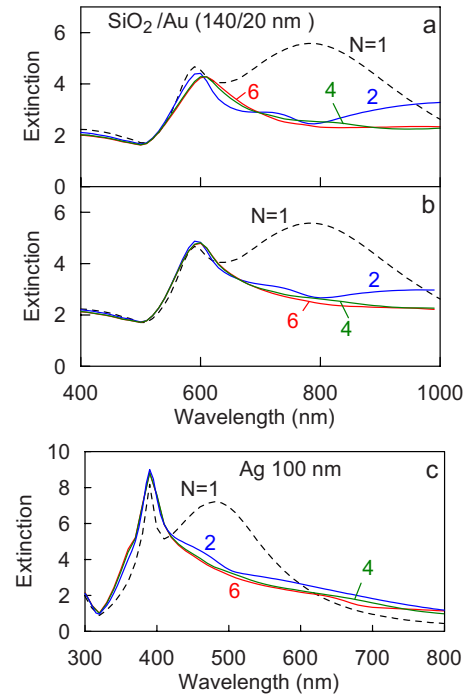


FIG. 5. (Color online) Extinction spectra for  $N \times N$  lattice clusters built up from [(a) and (b)]  $\text{SiO}_2/\text{Au}$  nanoshells (140/20 nm) and (c) silver 100 nm nanospheres.  $N=1, 2, 4,$  and 6. The interparticle-distance parameter  $s$  is 0.1 (a), 0.2 (b), and 0.5 (c).

### 4. Dependence of the monolayer-extinction spectrum on the particle number

The aim of this series of calculations was to determine the minimal monolayer-particle number for which the optical properties of the layer change insignificantly. Figure 5 gives examples of such calculations for lattice clusters built up from  $\text{SiO}_2/\text{Au}$  nanoshells with a core diameter of 140 nm and a gold-layer thickness of 20 nm and also for silver nanospheres with a diameter of 100 nm. The cluster numbers of particles  $N \times N$  were 1, 4, 16, and 36. From the results of the foregoing calculations, the interparticle-distance parameter  $s$  was chosen to be 0.1 and 0.2 for gold nanoshells and 0.5 for the silver spheres. One can clearly see the suppression of the dipole resonances for the nanoshells (near 800 nm) and silver spheres (near 490 nm) with a particle-number increase to 16. The calculated results for the silver lattice [Fig. 5(c)] are in very good qualitative agreement with the previous experiment.<sup>17</sup> The most important result of this series of calculations is that even a small  $4 \times 4$  cluster correctly represents the major optical properties of the monolayer, so that a particle-number increase from 16 to 36 changes little the general appearance of the spectra. This conclusion was accounted for in our further calculations.

### 5. Comparison of the extinction spectra of lattice and random monolayers

The foregoing conclusions were reached for a lattice model. Will they hold good for the more realistic model of random 2D particle arrays as well? This question is answered in Fig. 6, which compares the extinction spectra of lattice

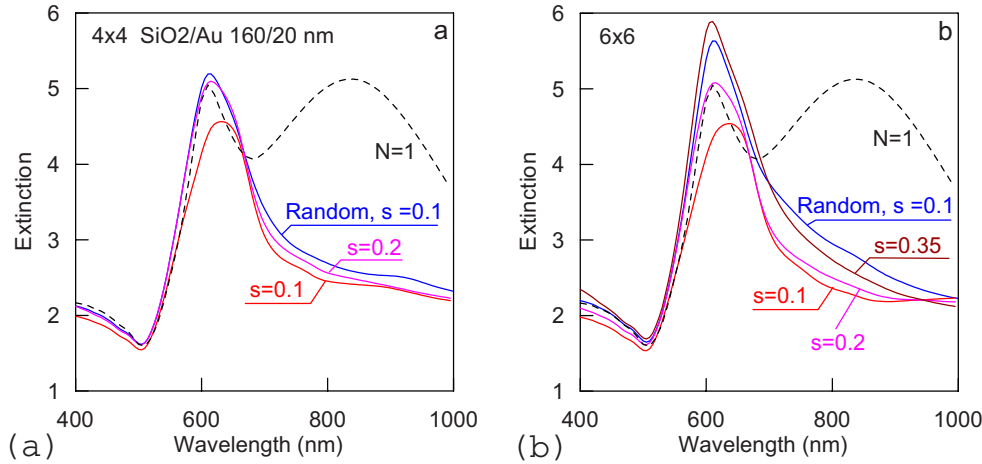


FIG. 6. (Color online) Comparison of the extinction spectra for lattice and random clusters made up of  $\text{SiO}_2/\text{Au}$  (160/20 nm) nanoshells with particle numbers of (a) 16 and (b) 36. Also shown are the spectra for isolated particles ( $N=1$ ). The interparticle-distance parameter is 0.1, 0.2, and 0.35 for the lattice clusters and 0.1 for the random clusters. The average particle density for the random clusters is (a) 0.415 and (b) 0.36 for 16 and 36 particles, respectively.

and random clusters with particle numbers of 16 and 36. The interparticle-distance parameter for a random cluster is fixed and is equal to 0.1. The average particle densities are 0.415 and 0.36 for 16-particle and 36-particle clusters, respectively. For the lattice clusters, the  $s$  parameter was considered as a fitting one, giving good agreement between the spectra. From the plots in Fig. 6, it can be seen that in both cases, the spectra for the lattice clusters with an  $s$  parameter of 0.2 are much the same as the spectra for the random clusters. Closer agreement between the spectra for the 36-particle clusters can be obtained if the  $s$  parameter is 0.35 in the lattice case.

### 6. Extinction, scattering, and absorption spectra for randomly structured monolayers

In the foregoing, we have analyzed only the extinction spectra. To gain an insight into the physical mechanisms responsible for suppression of the coupled dipole mode, one also has to investigate the influence of particle interactions on the cooperative absorption and scattering of light. In this section, we discuss the extinction, scattering, and absorption spectra for monolayers built up from randomly located silver particles and from silver and gold nanoshells with polystyrene cores. Although replacing silica cores with polystyrene ones changes little the optical properties of ensembles, we included this model in our calculations because particles of this type have also been studied previously in our experiments and others'.<sup>38</sup> With the results in Sec. IV taken into account, the particle number in a layer was chosen to be 36, and the average particle density varied between 0 (one particle) and 0.4.

Figure 7 shows the dependence of the extinction, scattering, and absorption spectra for random clusters of thirty-six 100 nm diameter silver particles on the average packing density. The calculated results were averaged over five independent cluster generations. As the particle density increases to 0.25, the dipole extinction band disappears, and we are left with only the quadrupole peak.

We now shift to consider separately the absorption and scattering spectra. Along with the dominant quadrupole resonance, there are two peaks corresponding to multipole excitations in the short-wavelength portion of the absorption spectrum. The contribution of absorption to the dipole ex-

inction band is negligible, so this band is determined entirely by dipole-resonance scattering. As the particle density increases, the structure of the absorption spectrum's short-wavelength portion changes little. By contrast, the scattering spectrum undergoes radical changes, showing suppression of dipole-resonance scattering. Thus, we get the important conclusion that the suppression in a monolayer of the dipole extinction band found by Malynych and Chumanov<sup>17</sup> is determined entirely by the decrease in *dipole-resonance scattering* that occurs when strongly scattering particles with a dipole and a quadrupole resonance move closer together. The electrodynamic interparticle interaction almost does not change the absorption spectrum, including its fine structure in the short-wavelength region.

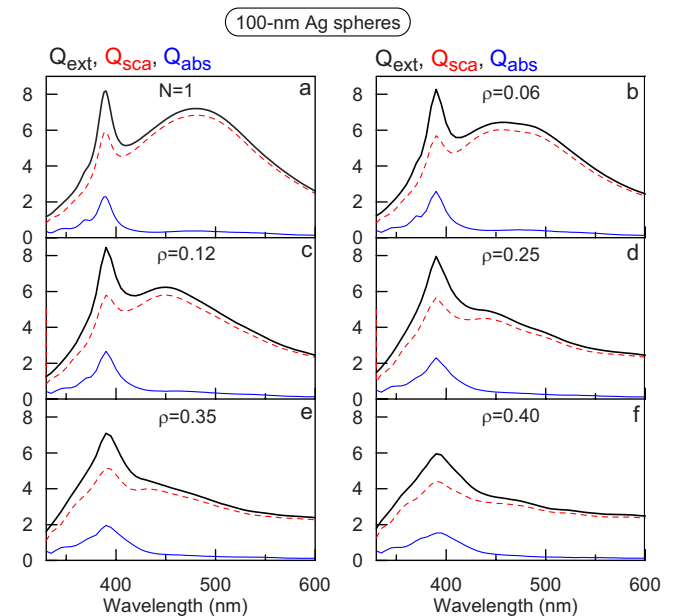


FIG. 7. (Color online) Extinction, scattering, and absorption spectra for random clusters made up of thirty-six 100 nm diameter silver particles. The minimal-distance parameter  $s$  is 0.05, and the average particle densities are (a) 0 (a single particle), (b) 0.06, (c) 0.12, (d) 0.25, (e) 0.35, and (f) 0.4. The calculated results were averaged over five statistical realizations.

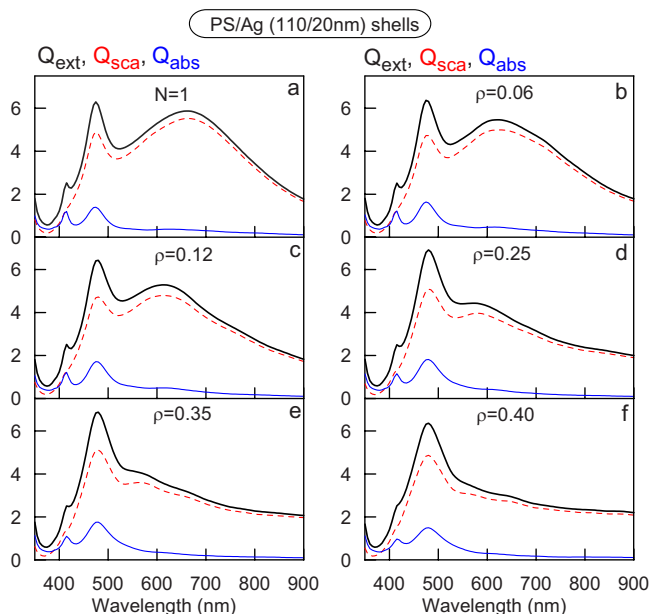


FIG. 8. (Color online) Extinction, scattering, and absorption spectra for random clusters made up of 36 PS/Ag-type silver nanoshells (core diameter of 110 nm; shell thickness of 20 nm). The minimal-distance parameter  $s$  is 0.05, and the average particle densities are (a) 0 (a single particle), (b) 0.06, (c) 0.12, (d) 0.25, (e) 0.35, and (f) 0.4. The calculated results were averaged over five statistical realizations.

Now, let us see how these conclusions depend on the parameters of the particles themselves. As an example, we use silver and gold nanoshells on polystyrene spheres. Figure 8 shows the spectra for a monolayer with the same parameters as in Fig. 7. The individual particles are 20 nm silver nanoshells on 110 nm polystyrene spheres. As in Fig. 7, all spectra were averaged over five cluster generations.

It can be seen that the transformation of the extinction, scattering, and absorption spectra occurring with increasing particle density in the monolayer is similar to that shown in Fig. 7. First, the clear-cut quadrupole and octupole absorption peaks in the short-wavelength portion of the spectrum almost do not depend on the average particle density in the monolayer. As in the case of solid silver spheres, the disappearance of the dipole extinction band is associated with the suppression of the dominant dipole-scattering band.

Figure 9 shows the results of calculations similar to those in Fig. 8 but concerning polystyrene (PS)/Au (110/35 nm) nanoshells. Distinct from the data in Fig. 8, the absorption spectrum in this system has a single quadrupole peak, the magnitude of which is comparable with the quadrupole contribution of scattering to total extinction. In fact, it is absorption that determines the total quadrupole extinction band, whereas the broad dipole band is determined entirely by scattering. Increasing the particle density results in an almost neutral scattering spectrum, so that the dipole extinction band disappears. This, again, is in agreement with the data of Figs. 7 and 8.

A more complex absorption spectrum for gold nanoshells is observed if the core diameter is increased to 200 nm and

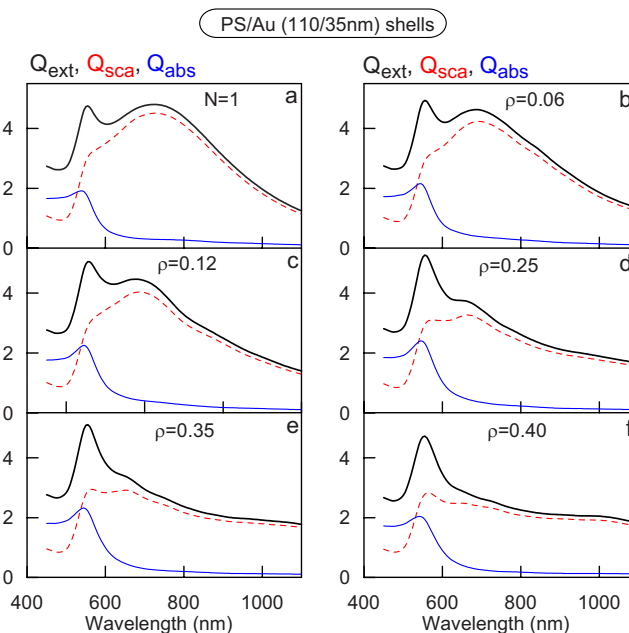


FIG. 9. (Color online) Same as in Fig. 7 but for PS/Au-type gold nanoshells (core diameter of 110 nm; shell thickness of 35 nm).

the layer thickness is decreased to 20 nm (Fig. 10). In such a case, the short-wavelength portion of the absorption spectrum demonstrates two multipole peaks, one of which coincides with the quadrupole extinction band. The broad dipole extinction band is determined by scattering, and the intensity of this band declines sharply with increasing particle density, as it also does in Figs. 7–9. As this takes place, the structure of the absorption spectrum remains the same.

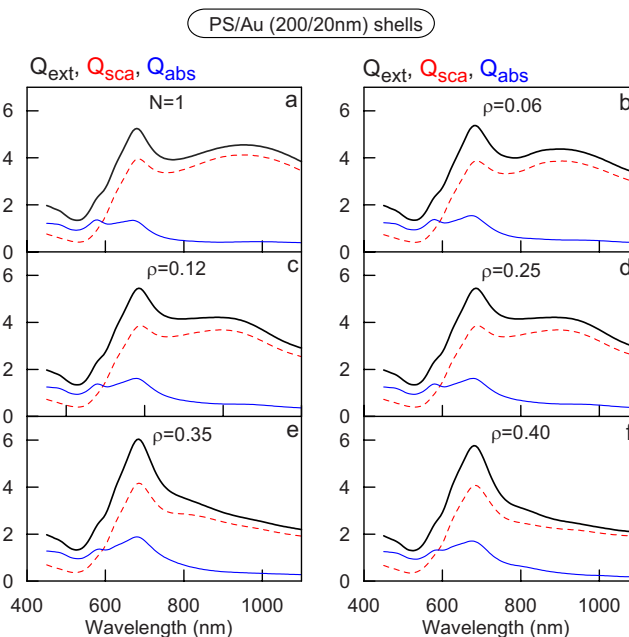


FIG. 10. (Color online) Same as in Fig. 8 but for gold nanoshells with a core diameter of 200 nm and a shell thickness of 20 nm.

### 7. Simple consideration based on a coupled dipole model

Although we are focused on the optics of interacting particles with dipole and quadrupole resonances, the physics of dipole-band suppression can be understood from a simple consideration based on a coupled dipole model. The total field exciting the  $i$ th monolayer particle can be found from a system of coupled equations,<sup>12</sup>

$$\mathbf{E}_i = \mathbf{E}_0 + \sum_{j \neq i} G_{ij} \mathbf{d}_j, \quad (13)$$

where  $\mathbf{E}_0 = \mathbf{e}_0 \exp(i\mathbf{k}_0 \mathbf{r}_i)$  is the incident field,  $\mathbf{d}_j$  is the dipole moment of the  $j$ th particle,  $G_{ij}$  is the well-known dipole-dipole interaction tensor,<sup>12(a)</sup>

$$G_{ij} = \left\{ \delta_{ij} - \frac{\mathbf{r}_{ij} \otimes \mathbf{r}_{ij}}{r_{ij}^2} + \left( 3 \frac{\mathbf{r}_{ij} \otimes \mathbf{r}_{ij}}{r_{ij}^2} - \delta_{ij} \right) \times \left( \frac{1}{k^2 r_{ij}^2} - \frac{i}{k r_{ij}} \right) \right\} \frac{\exp(ikr_{ij})}{kr_{ij}}, \quad (14)$$

$\mathbf{r}_{ij} = \mathbf{r}_i - \mathbf{r}_j$ , and  $\otimes$  denotes the dyadic product. To make an elementary estimation of the particle coupling effects, we apply a mean-field theory approach<sup>39</sup> by assuming

$$\mathbf{d}_j = \bar{\mathbf{d}} = \bar{d} \mathbf{e}_0 = \alpha \bar{E} \mathbf{e}_0, \quad (15)$$

where  $\bar{d}$  is the average dipole moment and  $\bar{E}$  is the average field amplitude. From Eqs. (14) and (15), we get  $\bar{\mathbf{d}} = \bar{\alpha} \mathbf{e}_0$ , where the average polarizability of a cluster particle is given by the relationships

$$\bar{\alpha} = \alpha / (1 - \alpha S), \quad (16)$$

$$S = \frac{1}{N} \sum_{\substack{i,j=1 \\ i \neq j}}^N (\mathbf{e}_0 G_{ij} \mathbf{e}_0). \quad (17)$$

After averaging Eq. (17) over the polarizations  $\mathbf{e}_0$ , we get

$$\bar{S} = \frac{1}{N} \sum_{\substack{i,j=1 \\ i \neq j}}^N \frac{1 - ikr_{ij} - kr_{ij}^2}{2r_{ij}^3} \exp(ikr_{ij}). \quad (18)$$

The ratio between single-particle and array-particle extinctions is equal to

$$C_{ext}^1 / C_{ext} = \text{Im}(\alpha) / \text{Im}(\bar{\alpha}) = |1 - \alpha \bar{S}|^2. \quad (19)$$

A numerical evaluation of the dipole sum  $\bar{S}$  [see, e.g., Refs. 22(c) and 22(d)] shows that the ratio in Eq. (19) becomes greater than 1 when the relative particle separation  $s$  decreases. A simple analytical estimation can be made for small arrays with  $kr_{ij} \ll 1$ :

$$\bar{S} = \frac{b}{d^3(1+s)^3}, \quad (20)$$

where the constant  $b$  is close to 1. Near the resonance wavelength of a single sphere, we have<sup>28</sup>  $\varepsilon = -2\varepsilon_m$ , and the sphere polarizability equals  $\alpha = (d/2)^3(1 + i3\varepsilon_m/\varepsilon'')$ . Finally, we arrive at the following relationship:

$$\frac{C_{ext}^1}{C_{ext}} = \left[ 1 - \frac{b}{8(1+s)^3} \right]^2 + \frac{9b^2}{64(1+s)^6} \frac{\varepsilon_m^2}{(\varepsilon'')^2}, \quad (21)$$

which predicts the array resonance suppression ( $C_{ext}^1 > C_{ext}$ ) and explains the strong dependence of the ratio in Eq. (21) on the interparticle separation parameter  $s$ .

## III. EXPERIMENT

### A. Materials and methods

#### 1. Nanoshell fabrication

The following reagents were used in synthetic procedures: tetraethyl orthosilicate (TEOS; Aldrich), 3-aminopropyltrimethoxysilane (APTMS; Aldrich), 3-mercaptopropyltrimethoxysilane (MPTES; Aldrich), tetrakis(hydroxymethyl)phosphonium chloride (THPC; Fluka), and aminated polystyrene spheres (diameters of 75, 100, and 150 nm; VNIISK, Russia). Tetrachloroauric acid (TCAA; Aldrich), caustic soda, potash (Reachim Co., Russia), and formaldehyde (Serva) were of research grade; 25% aqua ammonia was of analytical grade. Ethanol was purified by additional distillation. All experiments used triply distilled water.

Silica-gold nanoshells were fabricated as described,<sup>40</sup> with minor modifications in the reagent concentrations. First, silica nanoparticles were grown by reducing TEOS with  $\text{NH}_4\text{OH}$  in absolute ethanol. The particle surface was then functionalized with amine groups by reaction with APTMS in ethanol. For optimization of the attachment (or deposition) process, this colloid was aged for 2 days, and then the  $pH$  was adjusted to 4 with 0.2M  $\text{H}_3\text{PO}_4$ .

For the preparation of gold seeds, 220  $\mu\text{l}$  of 1M aqueous NaOH and 6  $\mu\text{l}$  of 80% THPC were added to 20 ml of triply distilled water. The solution was vigorously agitated on a magnetic stirrer at 1000 rpm, and 880  $\mu\text{l}$  of a 1% TCAA solution was added.

Next, aminated silica particles were added to the gold-seed suspension. Gold particles adsorb to the amine groups on the silica surface, resulting in a silica nanoparticle covered with the gold colloid. Silica/gold nanoshells were then grown by reacting  $\text{HAuCl}_4$  with the silica-colloid particles in the presence of formaldehyde at room temperature. This process reduces additional gold on the adsorbed colloid, which acts as nucleation sites. The nanoshells were centrifuged, concentrated tenfold, and sonicated in high-pressure-liquid-chromatography-grade water until use.

Gold nanoshells on polystyrene cores were synthesized similarly, except that synthesis of aminated silica nanoparticles was rejected and ready-made aminated polystyrene cores were used instead. The optical properties of suspensions of gold nanoshells on silica cores differ little from those for suspensions of gold nanoshells on polystyrene cores, but in our experiments, the quality of the spectra in the former case was higher than that in the latter case. This may have been due to the insufficient degree of polystyrene-particle amination in the samples obtained from the manufacturer. In the case of the silica particles, the degree of amination was checked in our synthetic protocol. Therefore, the

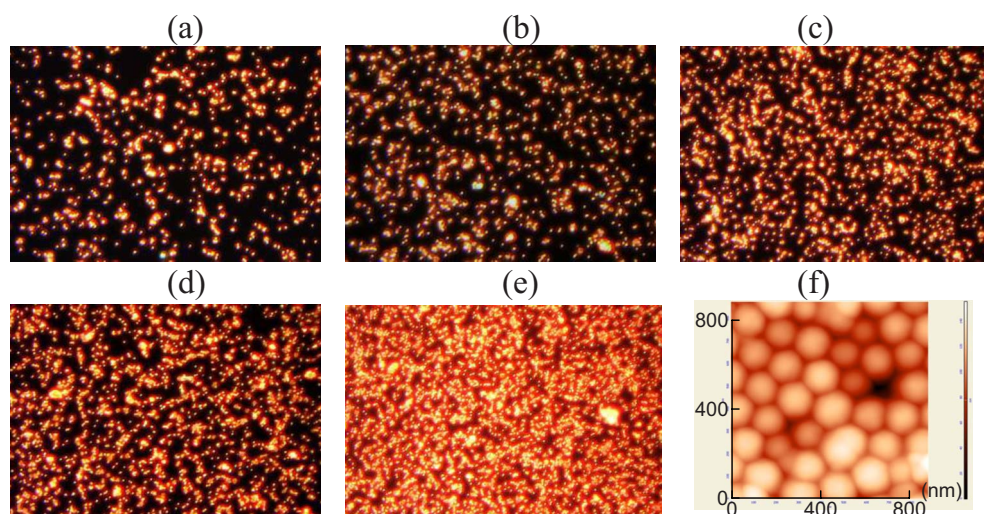


FIG. 11. (Color online) Dark-field microscopic images of glass-adsorbed 180 nm gold nanoshells. Incubation times: (a) 10 min, (b) 15 min, (c) 20 min, (d) 30 min, and (e) 60 min. (f) AFM image of a monolayer portion showing closely packed particles (incubation time of 12 h).

nanoparticle quality, assessed by the quality of the spectra, was higher. For these reasons, in what follows, we discuss the data only for nanoshells on silica.

## 2. Nanoshell monolayer fabrication

Before use, the glass or quartz substrates were submerged in a piranha solution for 30 min, rinsed well with de-ionized water and ethanol, and dried in a stream of nitrogen. The clean quartz substrates were immersed in a 10% (*v/v*) solution of MPTES in a 95:5 (*v/v*) ethanol/H<sub>2</sub>O mixture for 3 h. Subsequently, the substrates were removed from the silane solution, extensively rinsed with ethanol, and dried in a stream of nitrogen. The covalent binding of silane groups to the substrates was enhanced by promotion in a 105 °C oven for 10 min in nitrogen. The silane-functionalized quartz substrates were placed into 3 ml of a nanoshell suspension, and the suspension was kept shaking for different times (10 min to 12 h) to form a monolayer film. After the prescribed period, the substrates were removed from the nanoparticle suspension, rinsed copiously with H<sub>2</sub>O, and dried at room temperature.

## 3. Characterization

Scanning electron microscopy (SEM) images of silica particles, nanoshells, and monolayers were taken with a Philips XL30 field emission gun instrument operated at an accelerating voltage of 5–10 kV. Atomic force microscopy (AFM) images of nanoshell monolayers were taken with a Solver BIO instrument (NT-MDT, Russia).

UV-vis-NIR spectra were measured with a Specord M-40 (Carl Zeiss, Jena) and a Shimadzu UV-1601PC spectrophotometer. Dynamic light-scattering (DLS) measurements were made with a Zetasizer Nano ZS analyzer (Malvern, UK) and with a PotoCorr FS instrument (Photo Corr Inc., Russia).

## B. Results and Discussion

### 1. Kinetics of monolayer formation

Figure 11 shows dark-field images of 180 nm (outer di-

ameter) gold nanoshells adsorbed from the suspension to the functionalized glass in various incubation times. Visually, the observed intensity of resonance scattering in the red part of the spectrum allows an easy check on the change in particle density in the monolayer being formed. We note that extended incubation gives rise to multilayered aggregated structures whose optical spectra resemble the spectra for 3D aggregates.<sup>12</sup> To illustrate, in Fig. 11(f), we give an AFM image of the layer portion closely filled with 180 nm nanoshells after 12 h of incubation.

Figure 12 shows an enlarged portion of a SEM image for a 230 nm nanoshell monolayer. One can clearly see the hexagonal 2D structure of the monolayer. The average relative interparticle separation is about 0.1, with noticeable fluctuations indicating the random positions of the attached par-

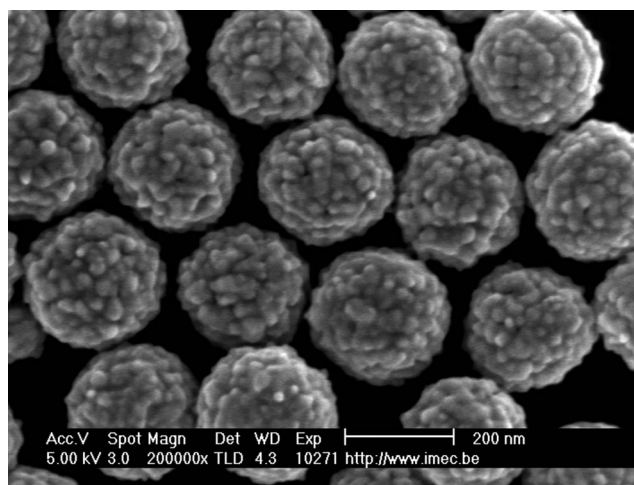


FIG. 12. SEM image of a monolayer portion showing self-assembled silica/gold nanoshells on a silane-functionalized quartz substrate. The average nanoparticle diameter is  $245 \pm 12$  nm (standard deviation, SEM data), and the average silica-core diameters are  $200 \pm 10$  nm (SEM data) and  $212 \pm 5$  nm (DLS data).

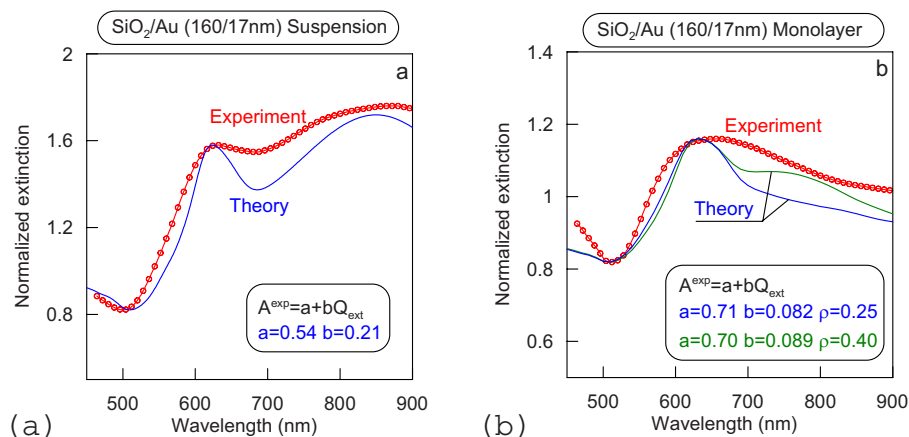


FIG. 13. (Color online) Normalized experimental and theoretical extinction spectra (a) for a gold-nanoshell suspension and (b) for a monolayer on a silane-functionalized glass substrate in water. The theoretical shell thickness (17 nm) was chosen from the best agreement between the suspension spectra and is close to the experimental value (20 nm, DLS data). The monolayer theoretical spectra were averaged for five independent generations of random arrays ( $N=36$ ), with the average surface particle densities  $\rho=0.25$  and  $0.4$  ( $s$  parameter of  $0.05$ ).

ticles. We also note the rough structure of the nanoshell surface, associated with preferential reduction of TCAA on the primary seeds attached.

## 2. Extinction spectrum for a nanoshell suspension and a two-dimensional layer: Comparison of theory with experiment

Figure 13(a) shows an experimental spectrum for gold nanoshells with a silica-core diameter of 160 nm and an average shell thickness of about 20 nm (data from DLS measurements). For comparison with theory, the following normalization procedure was used. With possible uncertainties associated with particle concentration and core-diameter and shell-thickness distributions taken into account and also considering the imperfection of the degree of shell filling with gold, we assumed that the experimental and theoretical spectra for an idealized monodisperse model are linearly related as follows:

$$A^{exp} = a + bQ_{ext}(d_{SiO_2}, \Delta d_{Au}), \quad (22)$$

where  $A^{exp}$  is the measured optical density and  $Q_{ext}$  is the theoretical extinction coefficient, depending on the core diameter and on the shell thickness. The  $a$  and  $b$  coefficients can be found from the requirements for spectra coincidence at two characteristic points. As such points, we chose a short-wavelength extinction minimum and the quadrupole maximum. The core-diameter and shell-thickness values were taken from the dynamic-scattering data, and the shell thickness was varied slightly around the DLS value so as to obtain the best agreement with experiment. In this way, we arrived at a theoretical model with the following values: shell thickness of 17 nm,  $a$  coefficient of 0.54, and  $b$  coefficient of 0.21. The theoretical curve in Fig. 13(a) shows a model spectrum that differs from the experimental one by the greater depth of the minimum between quadrupole and dipole bands. This difference can be attributed to several reasons, including particle polydispersity<sup>36</sup> and the imperfect rough gold surface.<sup>24,41</sup> Note that the dipole extinction peak is deter-

mined by scattering, whereas the quadrupole peak is related to both the absorption and the scattering contribution.

Figure 13(b) shows experimental and theoretical monolayer spectra for the same 160/17 nm nanoshells. The theoretical models correspond to random clusters built up from 36 particles with average densities of 0.25 and 0.4 (the spectra were averaged over five realizations). The spectra were normalized in the same way as in the suspension case. Before normalization, the experimental values of extinction were divided by the quadrupole peak. The corresponding normalization coefficients are given in the plots. Considering the many factors not accounted for in the theoretical model, we can say that the agreement between calculated and measured results is satisfactory. In any case, both theoretical and experimental spectra for the monolayer demonstrate suppression of the long-wavelength dipole-scattering mode.

We also synthesized  $SiO_2/Au$  nanoshells with an average core diameter of  $200 \pm 10$  nm and an outer average diameter of  $242 \pm 12$  nm (SEM data, Fig. 12). Accordingly, the gold-layer thickness was about 21 nm. However, the average DLS core diameter was about  $212 \pm 5$  nm, implying the average gold-layer thickness to be about 15 nm. For simplicity, these particles will be referred to as 200/20 nm nanoshells. We examined the single-particle and monolayer optical properties (Fig. 14). The core diameter and shell thickness were varied slightly around the SEM and DLS values so as to obtain the best agreement with experiment. In this way, we arrived at a theoretical model with an average core diameter of about 230 nm and a shell thickness of about 15 nm. For comparison with the experimental spectra, we used the same normalization as described above [Eq. (22)].

Calculations with fitting size parameters reproduce the spectral positions of both quadrupole and dipole bands. The quadrupole extinction peak for a particle suspension is located near 760 nm, and the dipole-scattering band lies in the near IR region (about 1100 nm). Moreover, in contrast to Fig. 13, the theoretical single-particle spectrum reveals an octupole resonance near 650 nm, which is not seen, however, in the experimental plots because of the polydispersity and surface roughness effects.<sup>41</sup> A separate calculation of extinc-

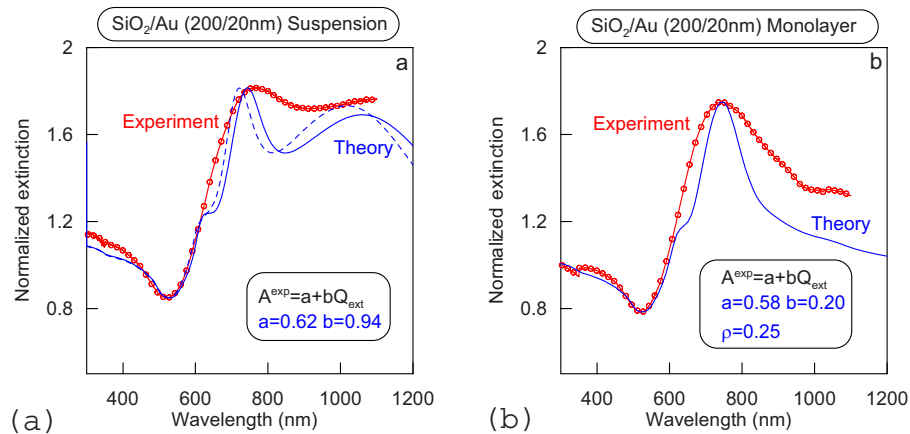


FIG. 14. (Color online) Normalized experimental and theoretical extinction spectra for a suspension of  $\text{SiO}_2/\text{Au}$  nanoshells (200/20 nm, SEM data) and for a monolayer on a silane-functionalized quartz substrate in water. The experimental monolayer extinction was multiplied by 6 before normalization, according to Eq. (22). The monolayer theoretical spectra were averaged for five independent generations of random arrays ( $N=36$ ), with the average surface particle density  $\rho=0.25$  (the  $s$  parameter equals 0.05). The fitting average core diameter and gold-shell thickness are 230 and 15 nm, respectively.

tion, absorption, and scattering spectra allows us to attribute the octupole peak to the dominant absorption resonance, the quadrupole peak to both the scattering and the absorption contribution, and the dipole peak to the dominant scattering resonance. The particle interaction in the experimental monolayer brought about a noticeable decrease in the extinction shoulder (800–1100 nm) because of suppression of the scattering resonance. To simulate the monolayer spectrum, we used the fitting average core diameter and gold shell thickness (230 and 15 nm) and five independent calculations for a random array ( $N=36$ ) with the average surface particle density  $\rho=0.25$  (the  $s$  parameter equals 0.05). In general, the model calculations agree well with the measured spectrum. It should be also noted that the theoretical single-particle octupole peak does not disappear for the coupled array particles.

We conclude this section with a comparison of our data with the recent observations by Wang *et al.* for nanoshell monolayers.<sup>19</sup> In contrast to our spectra (Figs. 13 and 14), those authors observed two distinct bands: a narrow visible (or NIR) band at wavelengths corresponding to the isolated nanoshell quadrupole plasmons and a new broad band extending from the near-infrared region well into the midinfrared region of the spectrum. The appearance of these bands was explained by a plasmon-hybridization model to multi-nanoparticle systems.<sup>24</sup> When nanoshells are closely packed in an array structure, the dipolar plasmons of the individual nanoshells strongly intermix to form a hybridized infrared plasmon band. On the other hand, the individual quadrupole resonances intermix rather weakly and give rise to a near-infrared plasmon band that is similar to the dipole plasmon of the individual nanoshells. Thus, our simulations and measurements demonstrated suppression of the coupled dipole band for interacting monolayer particles, whereas the data of Ref. 19 illustrated an increased NIR extinction due to the appearance of a new hybridized plasmon band. This discrepancy can be explained by the difference in structure between the arrays under examination. In our case, the nanoshells were well separated, as can be seen from the SEM images in Fig. 12. For such arrays, the interparticle coupling leads to

suppression of the dipole band, which can be explained with simple symmetry considerations,<sup>17</sup> the dipole coupling model [Eqs. (19) and (21)], or exact multipole simulations. The SEM images of closely packed arrays of Ref. 19 show a zero interparticle distance and, possibly, interparticle sintering. For such clusters, numerical simulations<sup>6,12</sup> and the plasmon-hybridization concept<sup>19</sup> predict the formation of a broad band evolved from the dipolar plasmon mode of individual particles.

### 3. Dependence of the monolayer quadrupole resonance on the external-medium refractive index

Malynych and Chumanov<sup>17(b)</sup> showed that the coupled-quadrupole-resonance wavelength of silver nanospheres in a polymer film is approximately dependent linearly on the refractive index of the external medium ( $m$ -cresol solutions),  $n_m$ . This property can be used in building sensors based on self-assembled layers of silver nanoparticles. In this section, we present experimental results for a gold-nanoshell monolayer on a glass substrate placed in media with different refractive indices. As such media, we used air, water, ethyl alcohol, hexane, carbon tetrachloride, and  $m$ -cresol solutions, with concentrations ranging from 0% to 80% ( $w/w$ ). The core diameter (190 nm) and gold-shell thickness (24 nm) were obtained from DLS measurements. The theoretical resonance wavelengths  $\lambda_q$  were calculated for a  $4 \times 4$  lattice with a relative-interparticle-distance parameter  $s$  of 0.2 and for external-medium refractive indices ranging from 1 to 1.7.

In general, the calculated resonance wavelength  $\lambda_q$  can be approximated by a straight line only roughly because the calculated relationship  $\lambda_q=f(n_m)$  was clearly nonlinear and the experimental points lie below the theoretical relationship (data not shown).

Earlier,<sup>42</sup> we showed that the relative shift in the plasmon resonance of individual particles,  $\Delta\lambda_p/\lambda_p$ , is related to the increment in the external-medium refractive index,  $\Delta n_m/n_m$ , by the following simple linear equation:

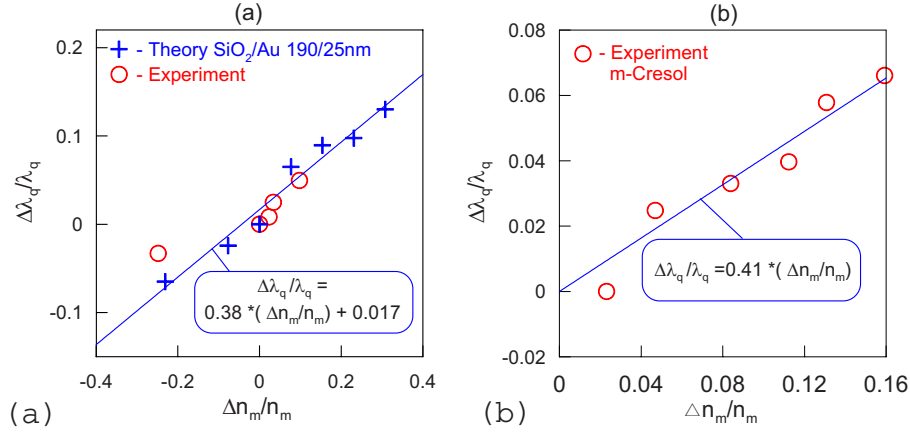


FIG. 15. (Color online) (a) Experimental (circles) and theoretical (crosses) dependences of the normalized quadrupole-resonance wavelength shift  $\Delta\lambda_q/\lambda_q$  on the normalized external-medium refractive index increment  $\Delta n_m/n_m$ . Calculations and measurements for  $\text{SiO}_2/\text{Au}$  (190/25 nm) nanoshell monolayer in air, water, ethyl alcohol, hexane, and carbon tetrachloride. (b) Experimental dependence of  $\Delta\lambda_q/\lambda_q$  on  $\Delta n_m/n_m$  for the same monolayer placed in water and solutions of *m*-cresol (0%, 20%, 40%, 60%, and 80%). The straight lines show a linear approximation of the (a) theoretical and (b) experimental data.

$$\frac{\Delta\lambda_p}{\lambda_p} = \frac{\Delta n_m}{n_m} \left( 1 - \frac{\lambda_0^2}{\lambda_p^2} \varepsilon_{ib} \right), \quad (23)$$

where  $\lambda_0$  is the wavelength of electronic plasma oscillations in vacuum and  $\varepsilon_{ib}$  is the contribution of interband transitions to the bulk dielectric function of the metal. Figure 15(a) presents theoretical and experimental data for the relative shifts in the quadrupole resonance,  $\Delta\lambda_q/\lambda_q$ , plotted as a function of the relative-refractive-index increment  $\Delta n_m/n_m$ . For definiteness, we chose a refractive index for water of 1.33 as a zero point of the spectral shift. The straight line shows a linear regression of the theoretical data:

$$\frac{\Delta\lambda_p}{\lambda_p} = 0.38 \frac{\Delta n_m}{n_m} + 0.017. \quad (24)$$

If a linear fit through the coordinate origin is used, the angular coefficient in Eq. (24) will be equal to 0.415. Using the tabulated<sup>25</sup> values for gold,  $\lambda_0=131$  nm and  $\varepsilon_{ib}=12.2$ , and also the resonance wavelength for water,  $\lambda_q=620$  nm, we find from Eq. (23) the angular-coefficient value of 0.455, which is close to the above estimates (0.382 and 0.415).

Figure 15(b) shows experimental points for the same monolayer in *m*-cresol solutions and a linear fit through the coordinate origin,

$$\frac{\Delta\lambda_p}{\lambda_p} = 0.42 \frac{\Delta n_m}{n_m}. \quad (25)$$

Again, there is satisfactory agreement with the angular-coefficient value of 0.455, predicted by Eq. (23).

Finally, it is of interest to compare our data with those obtained by measuring the coupled resonance shift of silver nanospheres embedded in a polymer film in *m*-cresol solutions. For the maximal refractive index increment  $\Delta n_m \approx 0.25$ , the maximal wavelength shift was about  $\Delta\lambda_q \approx 40$  nm. Therefore, the average sensitivity can be estimated as  $\Delta\lambda/\Delta n_m \approx 160$  nm/refractive index (RI), this being significantly higher than the sensitivity value for the gold-

nanoshell monolayer,  $\Delta\lambda/\Delta n_m \approx 100$  nm/RI. However, the relative shift obeys relation (25) with an angular slope of 0.48, which is very close to the gold-nanoshell case. Furthermore, substitution of the tabulated silver constants ( $\lambda_0 \approx 140$  nm,  $\varepsilon_{ib} \approx 5$ ) and the average quadrupole wavelength  $\lambda_q=450$  nm<sup>17</sup> into Eq. (23) gives an angular slope of 0.47, again, in excellent agreement with the experimental data. Thus, the simple universal relation Eq. (23) from Ref. 42 may be applicable not only to the dipole resonance of individual particles (for which it was derived) but also to the coupled quadrupole resonance of a 2D monolayer. Recently,<sup>43</sup> we found that Eq. (23) holds for multipole resonances in gold nanorods as well.

#### IV. CONCLUSIONS

In this work, we have examined the cooperative optical properties of monolayers of nanoparticles that, when isolated, have a dipole and a quadrupole plasmon resonance. Theoretical calculations have been done for 2D lattice and random clusters of spherical silver or gold particles and also for gold or silver nanoshells on silica or polystyrene cores. We have shown that effective suppression of the dipole extinction band is observed at an average interparticle distance of about 0.1–0.2 of the particle diameter for the lattice clusters and at an average particle-surface density of about 0.25 for the random monolayers. Calculations using a range of particle numbers showed that even clusters with a small particle number (about 16–36) correctly represent the main spectral properties of a monolayer. Although the spectra for the 2D lattice and random clusters differed in detail, the overall picture of spectrum transformation with increase in the particle-surface density was almost the same in both cases. Studying the absorption and scattering contributions to the total extinction spectra showed that the close particle proximity and particle coupling change little the absorption spectra, preserving their multipole resonances in the short-wavelength spectral region. The suppression of the long-

wavelength extinction band occurs wholly because of the suppression of the broad dipole-scattering resonance. Most likely, this effect is connected with the destructive field interference from the closely located particles.

We presented an experimental confirmation of dipole-resonance suppression for a monolayer of SiO<sub>2</sub>/Au-type nanoshells on a functionalized glass substrate. Our measurements and calculations of the spectral location of the quadrupole coupled resonance for a gold-nanoshell monolayer on a glass substrate in various immersion media showed the validity of the universal linear relation Eq. (23). It is notable that originally, relation (23) was obtained for the dipole resonance of isolated particles and subsequently was confirmed in the theory of multipole resonances of gold nanorods.

Thus, the rigorous theoretical modeling performed for dipole-quadrupole nanoparticles of various natures and the experimental verification of dipole-resonance suppression in a monolayer of nanoshells point to the general physical na-

ture of the effect first described in Ref. 17(a) for a monolayer of silver nanospheres. Moreover, the first exact multipole simulations of the particle-substrate coupling have shown its negligible contribution to the observed spectra, provided that the relative dielectric function of the interface is close to 1 (e.g., less than 1.5).

#### ACKNOWLEDGMENTS

This research was partly supported by grants from the Russian Foundation for Basic Research and from the Ministry of Science and Education of the Russian Federation, No. RNP.2.1.1.4473. B.N.K. was supported by grants from the President of the Russian Federation (No. MK 2637.2007.2) and INTAS YS (No. 06-1000014-6421). We thank D. N. Tychinin (IBPPM RAS) for help in the preparation of this paper.

\*Corresponding author: khlebtsov@ibppm.sgu.ru

- <sup>1</sup>C. R. Yonzon, X. Zhang, J. Zhao, and R. P. Van Duyne, *Spectroscopy* **22**, 42 (2007).
- <sup>2</sup>S. Kumar, N. Harrison, R. Richards-Kortum, and K. Sokolov, *Nano Lett.* **7**, 1338 (2007).
- <sup>3</sup>G. F. Paciotti, D. G. I. Kingston, and L. Tamarkin, *Drug Dev. Res.* **67**, 47 (2006).
- <sup>4</sup>X. Huang, I. H. El-Sayed, W. Qian, and M. A. El-Sayed, *J. Am. Chem. Soc.* **128**, 2115 (2006); D. Pissuwan, S. M. Valenzuela, and M. B. Cortie, *Trends Biotechnol.* **24**, 62 (2006); P. K. Jain, I. H. El-Sayed, and M. A. El-Sayed, *Nano Today* **2**, 16 (2007).
- <sup>5</sup>U. Kreibig and M. Vollmer, *Optical Properties of Metal Clusters* (Springer-Verlag, Berlin, 1995).
- <sup>6</sup>B. N. Khlebtsov, V. P. Zharov, A. G. Melnikov, V. V. Tuchin, and N. G. Khlebtsov, *Nanotechnology* **17**, 5167 (2006).
- <sup>7</sup>K.-S. Lee and M. A. El-Sayed, *J. Phys. Chem. B* **109**, 20331 (2005); P. K. Jain, K. S. Lee, I. H. El-Sayed, and M. A. El-Sayed, *ibid.* **110**, 7238 (2006); C. J. Noguez, *J. Phys. Chem. C* **111**, 3806 (2007).
- <sup>8</sup>V. A. Markel, *J. Mod. Opt.* **39**, 853 (1992); K.-H. Su, Q.-H. Wei, X. Zhang, J. J. Mock, D. R. Smith, and S. Schultz, *Nano Lett.* **3**, 1087 (2003); W. Huang, W. Qian, P. K. Jain, and M. A. El-Sayed, *ibid.* **7**, 3227 (2007).
- <sup>9</sup>B. N. Khlebtsov, A. G. Melnikov, V. P. Zharov, and N. G. Khlebtsov, *Nanotechnology* **17**, 1437 (2006).
- <sup>10</sup>V. A. Markel, *J. Mod. Opt.* **40**, 2281 (1993); *J. Phys. B* **38**, L115 (2005).
- <sup>11</sup>L. L. Zhao, K. L. Kelly, and G. C. Schatz, *J. Phys. Chem. B* **107**, 7343 (2003).
- <sup>12</sup>(a) V. A. Markel, V. M. Shalaev, E. B. Stechel, W. Kim, and R. L. Armstrong, *Phys. Rev. B* **53**, 2425 (1996); (b) N. G. Khlebtsov, L. A. Dykman, Ya. M. Krasnov, and A. G. Melnikov, *Colloid J.* **62**, 765 (2000); (c) A. Lazarides and G. C. Schatz, *J. Phys. Chem. B* **104**, 460 (2000).
- <sup>13</sup>N. G. Khlebtsov, A. G. Melnikov, V. A. Bogatyrev, and L. A. Dykman, in *Photopolarimetry in Remote Sensing*, NATO Science Series II: Mathematics, Physics, and Chemistry, edited by G. Videen, Ya. S. Yatskiv, and M. I. Mishchenko (Kluwer, Dordrecht, 2004), Vol. 161, p. 265.
- <sup>14</sup>A. Wei, e-*J. Surf. Sci. Nanotechnol.* **4**, 9 (2006); C. L. Haynes and R. P. J. Van Duyne, *J. Phys. Chem. B* **105**, 5599 (2001).
- <sup>15</sup>T. Okamoto and I. Yamaguchi, *Opt. Lett.* **25**, 372 (2000); M. Lahav, A. Vaskevich, and I. Rubinstein, *Langmuir* **20**, 7365 (2004).
- <sup>16</sup>J. C. Riboh, A. J. Haes, A. D. McFarland, C. Ranjit, and R. P. Van Duyne, *J. Phys. Chem. B* **107**, 1772 (2003); F. Frederix, J. M. Friedt, K. H. Choi, W. Laureyn, A. Campitelli, D. Mondelaers, G. Maes, and G. Borghs, *Anal. Chem.* **75**, 6890 (2003); N. Nath and A. Chilkoti, *ibid.* **76**, 5370 (2004).
- <sup>17</sup>(a) S. Malynych and G. Chumanov, *J. Am. Chem. Soc.* **125**, 2896 (2003); (b) *J. Opt. A, Pure Appl. Opt.* **8**, 144 (2006).
- <sup>18</sup>B. N. Khlebtsov, V. A. Khanadeyev, D. A. Verin, and N. G. Khlebtsov, *Proc. SPIE* **6536**, 653602 (2007).
- <sup>19</sup>H. Wang, J. Kundu, and N. J. Halas, *Angew. Chem., Int. Ed.* **46**, 9040 (2007).
- <sup>20</sup>M. C. Buncick, R. J. Warmack, and T. L. J. Ferrell, *J. Opt. Soc. Am. B* **4**, 927 (1987); G. A. Niklasson, P. A. Bobbert, and H. G. Craighead, *Nanostruct. Mater.* **12**, 725 (1999); B. Lamprecht, G. Schider, R. T. Lechner, H. Ditlbacher, J. R. Krenn, A. Leitner, and F. R. Aussenegg, *Phys. Rev. Lett.* **84**, 4721 (2000); V. Russier and M. P. Pileni, *Appl. Appl. Surf. Sci.* **162-163**, 644 (2000); S. Linden, A. Christ, J. Kuhl, and H. Giessen, *Appl. Phys. B: Lasers Opt.* **73**, 311 (2001).
- <sup>21</sup>G. B. Smith and V. N. Pustovit, *Opt. Commun.* **211**, 197 (2002).
- <sup>22</sup>(a) C. L. Haynes, A. D. McFarland, L. L. Zhao, G. C. Schatz, R. P. Van Duyne, L. Gunnarsson, J. Prikulis, B. Kasemo, and M. Kall, *J. Phys. Chem. B* **107**, 7337 (2003); (b) D. A. Genov, A. K. Sarychev, V. M. Shalaev, and A. Wei, *Nano Lett.* **4**, 153 (2004); (c) S. Zou, N. Janel, and G. C. Schatz, *J. Chem. Phys.* **120**, 10871 (2004); (d) S. Zou and G. C. Schatz, *ibid.* **121**, 12606 (2005); (e) A. Bouhelier, R. Bachelot, J. S. Im, G. P. Wiederrecht, G. Lerondel, S. Kostcheev, and P. Royer, *J. Phys. Chem. B* **109**, 3195 (2005); (f) M. Francoeur, P. G. Venkata, and M. P. Mengüç, *J. Quant. Spectrosc. Radiat. Transf.* **106**, 44

- (2007); (g) P. G. Venkata, M. Aslan, M. P. Mengüç, and G. Videen, *J. Heat Transfer* **129**, 60 (2007).
- <sup>23</sup>D. W. Mackowski, *J. Opt. Soc. Am. A* **11**, 2851 (1994).
- <sup>24</sup>D. W. Brandl, Ch. Oubre, and P. Nordlander, *J. Chem. Phys.* **123**, 024701 (2005).
- <sup>25</sup>N. G. Khlebtsov, V. A. Bogatyrev, L. A. Dykman, and A. G. Melnikov, *J. Colloid Interface Sci.* **180**, 436 (1996); B. N. Khlebtsov and N. G. Khlebtsov, *J. Quant. Spectrosc. Radiat. Transf.* **106**, 154 (2007).
- <sup>26</sup>P. B. Johnson and R. W. Christy, *Phys. Rev. B* **6**, 4370 (1972).
- <sup>27</sup>B. N. Khlebtsov and N. G. Khlebtsov, *J. Biomed. Opt.* **11**, 44002 (2006).
- <sup>28</sup>C. F. Bohren and D. R. Huffman, *Absorption and Scattering of Light by Small Particles* (Wiley, New York, 1983).
- <sup>29</sup>Z. C. Wu and Y. P. Wang, *Radio Sci.* **26**, 1393 (1991).
- <sup>30</sup>Y.-L. Xu, *J. Opt. Soc. Am. A* **20**, 2093 (2003); Y.-L. Xu and N. G. Khlebtsov, *J. Quant. Spectrosc. Radiat. Transf.* **79-80**, 1121 (2004).
- <sup>31</sup>G. Videen, *J. Opt. Soc. Am. A* **8**, 483 (1991); **9**, 844(E) (1992).
- <sup>32</sup>D. W. Mackowski, *J. Quant. Spectrosc. Radiat. Transf.* **109**, 770 (2008).
- <sup>33</sup>T. Wriedt and A. Doicu, *Opt. Commun.* **152**, 376 (1998).
- <sup>34</sup>P. Denti, F. Borghese, R. Saija, E. Fucile, and O. I. Sindoni, *Appl. Opt.* **16**, 167 (1999).
- <sup>35</sup>E. Eremina, Yu. Eremin, and Th. Wriedt, *Opt. Commun.* **246**, 405 (2005); **267**, 524 (2006); **273**, 278 (2007).
- <sup>36</sup>B. N. Khlebtsov, V. A. Bogatyrev, L. A. Dykman, and N. G. Khlebtsov, *Opt. Spectrosc.* **102**, 233 (2007).
- <sup>37</sup>H. Xu and M. Käll, *Sens. Actuators B* **87**, 244 (2002).
- <sup>38</sup>A. G. Dong, Y. J. Wang, Y. Tang, N. Ren, W. L. Yang, and Z. Gao, *Chem. Commun. (Cambridge)* **2002** 350; C. Song, D. Wang, Y. Lin, Z. Hu, G. Gu, and X. Fu, *Nanotechnology* **15**, 962 (2004); S. Weili, Y. Sahoo, M. T. Swihart, and P. N. Prasad, *Langmuir* **21**, 1610 (2005).
- <sup>39</sup>M. V. Berry and I. C. Percival, *Opt. Acta* **33**, 577 (1986).
- <sup>40</sup>S. J. Oldenburg, R. D. Averitt, S. L. Westcott, and N. Halas, *Chem. Phys. Lett.* **288**, 243 (1998).
- <sup>41</sup>K. E. Peceros, X. Xu, S. R. Bulcock, and M. B. Cortie, *J. Phys. Chem. B* **109**, 21516 (2005); H. Wang, G. P. Goodrich, F. Tam, C. Oubre, P. Nordlander, and N. J. Halas, *ibid.* **109**, 11083 (2005).
- <sup>42</sup>A. V. Alekseeva, V. A. Bogatyrev, B. N. Khlebtsov, A. G. Melnikov, L. A. Dykman, and N. G. Khlebtsov, *Colloid J.* **68**, 661 (2006).
- <sup>43</sup>B. N. Khlebtsov and N. G. Khlebtsov, *J. Phys. Chem. C* **111**, 11516 (2007).